



Rapid and reliable assessment of methane impacts on climate

Ilissa B. Ocko¹, Vaishali Naik² and David Paynter²

¹Environmental Defense Fund, Washington DC, 20009, USA

²NOAA Geophysical Fluid Dynamics Laboratory, Princeton, 08540, USA

5 *Correspondence to:* Ilissa B. Ocko (iocco@edf.org)

Abstract. It is clear that the most effective way to limit global temperature rise and associated impacts is to reduce human emissions of greenhouse gases, including methane. However, quantification of the climate benefits of mitigation options are complicated by the contrast in the timescales at which short-lived climate pollutants, such as methane, persist in the atmosphere as compared to carbon dioxide. Whereas simple metrics fail to capture the differential impacts across all timescales, sophisticated climate models that can address these temporal dynamics are often inaccessible, time-intensive, and require special infrastructure. Reduced-complexity models offer an ideal compromise in that they provide quick, reliable insights into the benefits across types of climate pollutants using basic knowledge and limited computational infrastructure. In this paper, we build on previous evaluations of the freely-available and easy-to-run reduced-complexity climate model MAGICC by confirming its ability to reproduce temperature responses to historical methane emissions. By comparing MAGICC model results to those from the reference GFDL CM3 coupled global chemistry-climate model, we build confidence in using MAGICC for purposes of understanding the climate implications of methane mitigation. MAGICC can easily and rapidly provide robust data on climate responses to changes in methane emissions.

1 Introduction

20 Reduced-complexity climate models offer an ideal framework for evaluating greenhouse gas mitigation options if they can accessibly and rapidly reproduce the results of more complex global chemistry-climate models (CCMs) (Meinshausen et al., 2011a). However, there is a critical need to build confidence in the ability of reduced-complexity models to simulate temperature responses to individual greenhouse gases rather than just the suite of climate pollutants, because greenhouse gases have vastly different radiative properties and atmospheric lifetimes (Myhre et al., 2013; Fiore et al., 2015); it is important to confirm that individual species are represented appropriately if reduced-complexity models are to serve as an effective tool for assessing climate benefits of mitigation actions. This is especially central for the analysis of methane (CH₄) mitigation actions, of which the climate policy community has been increasingly interested in pursuing (e.g., Alvarez et al., 2012; Shindell et al., 2012). Therefore, this paper builds on previous evaluations by comparing forcing and temperature responses to historical methane and carbon dioxide (CO₂) concentrations from a widely-used reduced-complexity climate model, with that from a



state-of-the-art coupled global chemistry-climate model. We ultimately seek to determine if a reduced-complexity climate model can be a useful and reliable tool for rapid assessment of methane mitigation measures.

Given that climate change impacts have now been observed on every continent and in every ocean (Stocker et al., 2013), reducing near- and long-term anthropogenically caused warming is urgent. While limiting long-term climate warming requires drastically reducing CO₂ emissions, reducing emissions of short-lived climate pollutants (SLCPs)—specifically, methane and black carbon (BC)—have been identified as one of the most effective ways to reduce near-term warming (e.g., Ramanathan and Xu, 2010; Shindell et al., 2012; Rogelj et al., 2013; Shoemaker et al., 2013). Methane emissions in particular account for a quarter of the excess energy trapped by human emissions, and today's anthropogenic methane emissions will have a larger impact on near-term warming than today's fossil fuel CO₂ emissions (Myhre et al., 2013 and references therein; IEA, 2015; Etminan et al., 2016). Sustained methane emissions will also impact long-term warming (Allen et al., 2016). Furthermore, reducing methane emissions has air quality and health co-benefits (West et al., 2013; Zhang et al., 2016; Melvin et al., 2016).

Most methane mitigation measures are assessed as a comparison to carbon dioxide warming impacts; almost all policy analyses rely on the simple metric Global Warming Potential (GWP) because of its simplicity and ease of use (Ocko et al., 2017). However, GWP is limited in its ability to quantify climate effects because it relies on the integrated impact of a pulse of emissions over a specified time horizon. Because methane and CO₂ have vastly different atmospheric lifetimes, their respective climate impacts occur over different timescales, and GWP is incapable of capturing these important temporal distinctions (e.g., Solomon et al. 2010; Alvarez et al., 2012).

Assessment of SLCP climate impacts over different timescales can be performed using comprehensive global chemistry-climate models (CCMs), however, a full assessment of various SLCP mitigation scenarios using sophisticated CCMs is computationally intensive and time-consuming. Determining robust climate responses to a specific mitigation scenario using CCMs require a large number of ensemble simulations (Deser et al., 2012), and forcing perturbations of specific mitigation scenarios are often too small for the response signal to be detected among internal climate variability. Further, many institutions do not have access to CCMs nor the technical capacity or expertise to run these models. Therefore, they must rely on partnerships with modeling centers that are often focused on model development. This reinforces the use of the simple GWP metric.

To avoid the need for the tremendous amount of computational resources required to perform CCM simulations and to rapidly provide scientific guidance for mitigation decisions, one option is to use reduced-complexity climate models. While detailed assessment of regional climate responses can only be provided by complex CCMs, the simpler models are ideal for analyzing global average climate responses, because they are easily accessible and quick. One such model is the freely available Model for the Assessment of Greenhouse-gas Induced Climate Change (MAGICC), initially developed in the late 1980s (Wigley and Rapper, 1987, 1992) and routinely updated since (e.g., Meinshausen et al., 2011a). While not meant to replace atmosphere-ocean global climate models (AOGCMs) and carbon cycle models, MAGICC is a complementary, computationally-



inexpensive tool that is capable of efficiently analyzing basic climate responses (such as radiative forcing, surface air temperature, and ocean heat uptake) to a suite of emission scenarios. Confidence in MAGICC results comes from a comprehensive effort to match several AOGCMs and carbon cycle models (Meinshausen et al., 2008, 2011a). Evaluations show that MAGICC closely reproduces temperature responses to aggregated forcings from the sophisticated Coupled Model
5 Intercomparison Project CMIP3 atmosphere-ocean and C4MIP carbon cycle models (Meinshausen et al., 2011c).

The reduced complexity model MAGICC is therefore a great resource for mitigation analysis where numerous scenarios exist and need to be evaluated before decision-making. To build confidence in MAGICC's evaluation of greenhouse gas mitigation strategies, we need to adequately assess its ability to reproduce climate responses to individual greenhouse gases beyond the aggregated forcings. Here, we analyze the capability of MAGICC in simulating climate responses to historical increases (1860-
10 2014) in methane and CO₂ by comparing the results with that from a state-of-the-art coupled chemistry-climate model, the National Oceanic and Atmospheric Administration (NOAA) Geophysical Fluid Dynamics Laboratory (GFDL) CM3 model, which has been shown to adequately reproduce historical temperature trends (Golaz et al. 2013, Griffies et al., 2011; Donner et al., 2011; Winton et al., 2012; John et al., 2012; Levy et al., 2013).

Our goal is to build confidence in the simulation of the climate response to methane in order to justify future use of MAGICC
15 to assess the climate impact of methane emissions mitigation scenarios. We add to previous evaluations by showing a high correlation between CM3's and MAGICC's radiative forcing and surface air temperature responses to changes in either CO₂ or methane in isolation, thereby strengthening confidence in MAGICC's simulation of climate responses to individual greenhouse gases with vastly different radiative properties and lifetimes.

2 Models and Simulations

20 2.1 MAGICC model description

We use MAGICC v.6 version developed in 2011 (<http://www.magicc.org/download>). MAGICC represents the complex coupled carbon-cycle climate system as a hemispherically averaged upwelling-diffusion ocean coupled to an atmosphere layer and a globally averaged carbon cycle model. The atmosphere has four boxes (one over land and one over ocean for each hemisphere) and is coupled to the mixed layer of the ocean hemispheres. The default number of ocean layers in each
25 hemisphere is 50 including the mixed layer (though users can select the number of levels), and heat exchange is driven by vertical diffusion and advection. The terrestrial carbon cycle model is a globally integrated box model with one living plant box and two dead biomass boxes (one for detritus and one for organic matter in soils). The terrestrial carbon cycle does not feedback into carbon dioxide concentrations in the atmosphere. The sea-to-air carbon flux is determined by the partial pressure differential for carbon dioxide between the atmosphere and surface layer of the ocean.



From 1765–2005, the MAGICC v.6 radiative forcing is driven by global-mean concentrations of greenhouse gases (carbon dioxide, methane, nitrous oxide, ozone-depleting substances and their replacements); prescribed regional direct aerosol radiative forcings (sulfate, black and organic carbon, sea salt, mineral dust); land-use, volcanic, and solar radiative forcings; prescribed black carbon on snow radiative forcings; emissions of tropospheric ozone precursors (carbon monoxide, nitrogen oxides, non-methane volatile organic carbon); and indirect (first and second) aerosol forcings calculated from prescribed regional aerosol optical depths (parameterizations described in detail in Meinshausen et al. (2011a)). For 2006 to 2014, the model is driven by emissions of gases and aerosols taken from the Representative Concentration Pathway (RCP8.5) scenario to capture a business-as-usual trajectory. Climate responses (such as surface air temperature) are provided as global annual averages and also across four spatial boxes (over land and ocean and by hemisphere).

Historical greenhouse gas concentrations are from Meinshausen et al. (2011b); prescribed aerosol forcings and land-use historical forcings are from the National Aeronautics and Space Administration (NASA) GISS model (<http://data.giss.nasa.gov/>); solar irradiance is provided by Lean et al. (2010); and historical emissions of ozone precursors are from Lamarque et al. (2010). Present-day (2005–2014) forcings are driven by emissions of gases and aerosols, and are taken from the Representative Concentration Pathway (RCP8.5) scenario to capture a business-as-usual trajectory. Carbon dioxide and methane radiative forcings are calculated using standard simplified expressions (Shine et al. 1990; Myhre et al. 1998).

For the most recent version of MAGICC, seven key climate parameters were calibrated to match 19 AOGCMs used in the Intergovernmental Panel on Climate Change (IPCC) Fourth Assessment Report AR4 (see Meinshausen et al., 2011a). The parameters include: equilibrium climate sensitivity, land-ocean warming ratio at equilibrium, vertical diffusivity in the ocean, sensitivity of feedback factors to radiative forcing change, sensitivity of vertical diffusivity at mixed layer boundary to global-mean surface temperatures (i.e., thermal stratification), land-ocean heat exchange coefficient, and an amplification factor for the ocean to land heat exchange. The MAGICC parameter set that best reproduces surface air temperatures and heat uptake of each AOGCM is determined via an optimization routine with 1000 iterations to find the combination that minimizes the squared differences between low-pass filtered time series. The effective climate sensitivities in MAGICC v.6 vary over time due to spatially non-homogenous varying feedbacks, until they reach the equilibrium climate sensitivity. The equilibrium climate sensitivity input into MAGICC depends on which AOGCM calibration is used; they range from 1.9 to 5.73 across all 19 models, with a mean (median) of 2.88 (2.59). Multi-model-ensembles are generated by running each simulation for all 19 AOGCM calibrations.

While the MAGICC model is particularly well-calibrated to more sophisticated models, the realism of MAGICC results relies on the realism of GCMs, which have their own sets of limits and uncertainties. Further limitations of MAGICC include incomplete knowledge of forcing patterns, unknown responses outside of the calibrated range, limited set of climate responses evaluated (such as temperature and heat uptake but not precipitation), reliance on a high level of parametrization (such as cloud feedbacks tuned to match those of more sophisticated GCMs), and possible errors in the data used for calibration. However,



despite these limitations, MAGICC has been shown to reasonably reproduce climate responses to all-forcing scenarios (Meinshausen et al., 2011a).

2.2 CM3 model description

We employ the GFDL global coupled atmosphere-ocean-chemistry model (GFDL-CM3; Donner et al., 2011; Griffies et al.,
5 2011) to assess the climate response to historical changes in methane and CO₂. CM3 uses a finite-volume dynamical core on
a cubed-sphere horizontal grid composed of six faces; each face includes 48 × 48 grid cells. The size of the grid cells range
from 163 km at the corners to 231 km near the face centers. In the vertical, the model domain extends from the surface up to
0.01 hPa (86 km) with 48 vertical hybrid sigma pressure levels. The model simulates tropospheric and stratospheric chemistry
interactively over the full vertical domain, with simulated ozone and aerosols influencing radiation calculations (Naik et al.,
10 2013; Austin et al., 2013). Ensemble members are generated by employing different sets of initial conditions (discussed in
more detail in Sect. 2.3.)

Global mean concentrations of well-mixed greenhouse gases (WMGHGs), including carbon dioxide nitrous oxide, methane,
and ozone-depleting substances (ODSs) are specified for radiation calculations for the historical period (1860-2005) from
Meinshausen et al. (2011b) and for the period 2006 to 2014 following the Representative Concentration Pathway (RCP8.5)
15 scenario. Within the chemistry module, global mean concentrations of methane are prescribed at the surface as lower boundary
condition and are allowed to undergo chemistry everywhere else in the model domain. Radiation calculations do not see the
full three-dimensional methane field (simulated in the chemistry module) and only employ the global-mean concentrations,
however, changes in ozone and water vapor are seen by the radiation. CM3 does not capture the indirect feedbacks on carbon
dioxide from methane.

20 CM3 is forced with emissions of short-lived species including ozone precursors, and aerosols and their precursors, volcanic
aerosols, solar radiation, and land-use change as described in detail by Donner et al. (2011) and Naik et al. (2013).
Anthropogenic emissions, including from biomass burning and ships, for the time period 1860–2005 are from the dataset of
Lamarque et al. (2010) developed in support of the Couple Model Intercomparison Project Phase 5 (CMIP5). For years 2006–
2014, anthropogenic emissions follow the RCP8.5 scenario. Natural emissions of all precursor species, except isoprene, are
25 included as described by Naik et al. (2013). Biogenic isoprene emissions are calculated interactively, as described by Lin et
al. (2012), based on the Model of Emissions of Gases and Aerosols in Nature (MEGAN) (Guenther et al., 2012).

CM3 includes explicit representation of both the direct and indirect aerosol effects on radiation. For the calculation of the
direct effect of aerosols on radiation, physical and optical properties of sulfate, black carbon, organic carbon, sea salt, and dust
are considered in the model (Donner et al., 2011). Sulfate and black carbon are assumed to be internally mixed while all other
30 aerosols are assumed to be externally mixed for radiation calculations. To account for the indirect effect of aerosols via aerosol-
water cloud interactions, the model treats water soluble aerosols, including sea salt, and organic aerosols as cloud-condensation



nuclei (CCN) allowing a physically based parameterization of CCN activation (Ming et al., 2006). The model does not consider the reduction in surface albedo caused by the deposition of BC on snow-covered surfaces.

2.3. Simulations

Four historical simulations are run for both MAGICC and GFDL CM3 to derive climate responses to isolated CO₂ and methane concentrations, respectively, and to parse out direct from indirect warming effects of methane. MAGICC was run from 1750 to 2100 by default, and CM3 was run from 1860 to 2014. As shown in Table 1, the direct runs for both models include an all-forcing simulation with all forcings varying with time except land-use; a simulation with CO₂ concentrations held at 1860 levels; and a simulation with methane concentrations held at 1860 levels. Subtracting temperature responses of the two latter runs from the former yield CO₂-only and methane-only climate responses, respectively (see Eqs. (1) and (2)). The same equations hold for the forcings as well.

$$\Delta T_{CO_2} = T_{All-forcing} - T_{CO_2=1860}, \quad (1)$$

$$\Delta T_{CH_4} = T_{All-forcing} - T_{CH_4=1860}, \quad (2)$$

For MAGICC, each simulation is run for all 19 AOGCM-calibrated configurations; each 350-year integration took approximately one second to run on a modern PC with a three GHz CPU processing speed. We use default MAGICC gas and aerosol properties, but update methane and tropospheric ozone radiative efficiencies and methane atmospheric lifetime to IPCC Fifth Assessment Report (AR5) values (Myhre et al., 2013; Stevenson et al., 2013) to reflect the latest science. However, we do not include newer estimates of methane radiative efficiency that account for shortwave absorption in addition to longwave absorption (Etminan et al., 2016) to be consistent with the CM3 model that only includes longwave effects. Including the shortwave component increases methane's radiative efficiency by over 20%. Further, we specifically do not tune MAGICC model climate and forcing properties to match that of CM3 because we are assessing how a "standard version" of the reduced-complexity climate model compares with CM3; the goal is not to match MAGICC to CM3 but to assess whether a downloaded version of MAGICC broadly behaves similar to CM3.

The set-up of GFDL-CM3 simulations conducted here was similar to that adopted for simulations performed in support of the CMIP5, except we obtained initial conditions from a longer preindustrial control (3000 years). Three-member ensembles of transient CM3 simulations were performed with each ensemble member initialized at different points in the preindustrial control simulation. Each 155-year integration of CM3 took about 15 days to complete on the NOAA's Remotely Deployed High Performance Computing System (RDHPCS) machine known as "Gaea" running on 464 processors.

To compute CM3 radiative forcings for CO₂ and methane (direct and indirect) that are closest to the definition used by MAGICC (the forcing at the tropopause after stratospheric temperature adjustment), we performed simulations with the



atmosphere-only version of CM3—AM3. The model configuration of AM3 was exactly the same as CM3 except AM3 model integrations over the period 1870 to 2014 were performed with observed sea-surface temperature and sea-ice cover (Rayner et al., 2003). Through the additional AM3 simulations, we were able to diagnose transient effective radiative forcing (ERF) (the change in net radiation balance at the top-of-atmosphere (TOA) following a perturbation to the climate system taking into account any rapid adjustments (Myhre et al., 2013)) due to CO₂ and methane. Transient ERF calculated in this way follow the proposed protocol for the AerChemMIP (Collins et al., 2016). While ERF calculated in this way eliminates the need to perform multiple time-slice integrations to assess the trends, it does not reflect the dependence of methane forcing on nitrous oxide concentration due to spectral overlap and likely underestimates the methane ERF (Forster et al., 2016).

To separate the effect of methane due to its influence on ozone and water vapor (indirect effects) from its effect on radiation (direct effect), we ran two simulations for MAGICC with methane chemistry turned off (an all-forcing run and methane held at 1860 levels run with methane chemistry turned off for both), and a simulation for AM3 with methane radiation calculations held constant beyond 1860. Equations (3) and (4), respectively, show how the indirect methane forcings were calculated for both the MAGICC and CM3 models.

$$\Delta F_{CH_4,indirect (MAGICC)} = F_{CH_4} - (F_{All-forcing,no\ chemistry1860} - F_{CH_4=1860,no\ chemistry}), \quad (3)$$

$$\Delta F_{CH_4,indirect (CM3)} = F_{CH_4 radiation=1860} - F_{CH_4(radiation+chemistry)=1860}, \quad (4)$$

The global mean historical concentrations of CO₂ and methane used to drive both models are shown in Fig. 1. Results for both models are presented as an average of the individual ensemble members. Surface air temperatures are taken to be 2 meters above the surface. For both models, we calculate temperature changes as the difference between temperatures in year *t* compared to that in 1860. A key difference between CM3 and MAGICC is CM3's internally generated unforced variability, driven by dynamics of heat exchange within the ocean-atmosphere-land system and internal influences on the energy budget. Therefore, we employ a five-year smoothing average to CM3 results to filter out some of the internal variability.

3 Results and Discussion

Figure 2 shows the global-mean top-of-atmosphere (TOA) radiative forcings (RF) in response to the all-forcing scenario as well as forcings attributed to isolated CO₂ and methane concentrations, respectively. Note that AM3 forcings include rapid adjustments in the troposphere in addition to the stratosphere, and therefore are considered an effective RF, while MAGICC derived RF only considers stratospheric temperature adjustment. MAGICC methane and CO₂ isolated forcings are much smoother than that of AM3 because of the lack of unforced variability in MAGICC. However, despite the slightly different forcing definitions and the unforced variability in AM3, all results are strongly correlated between AM3 and MAGICC (All-forcing $r^2 = 0.81$, CO₂-only $r^2 = 0.96$, CH₄-only $r^2 = 0.93$).



In the present-day (model year 2014), AM3 and MAGICC yield an all-forcing RF of 2.0 and 2.5 W m⁻², respectively; note that land use is held constant in this analysis. This is consistent with the IPCC (2013) values that show an all-forcing effective RF of 2.3 W m⁻² in 2011 (Myhre et al., 2013). The magnitudes for the CM3 and MAGICC all-forcing radiative forcings are slightly offset after 1960 (-1 W m⁻² in 1960). This is due to AM3's strong aerosol indirect forcing (Golaz et al., 2010) beginning around
5 this time when aerosol emissions in the mid-latitudes increased rapidly (Lamarque et al., 2010).

Isolating CO₂ and methane's contribution to overall forcings, MAGICC reasonably reproduces the forcing evolutions throughout the 20th Century as compared to AM3, and present-day forcings are consistent with the IPCC (2013) forcings attributed to CO₂ and methane emissions (1.68 and 0.97 W m⁻² in 2011, respectively) (Myhre et al., 2013). In MAGICC, methane's RF is consistently around half the value of that by CO₂. In AM3, methane's RF is much closer to that of CO₂ until
10 the year 2000 and beyond where they diverge. Before 1950, the difference between methane's RF in MAGICC vs. AM3 is consistent with internal variability, but after 1950, AM3's methane forcing exhibits a large increase not captured by MAGICC. AM3 also shows a slight decrease in methane RF around the year 2000 through 2005, consistent with global concentrations remaining flat for about a decade in the mid-1990s to early 2000s, before rapidly increasing from 2007 onwards (Fig. 1).

Methane's role in radiative forcing can be divided into direct contributions via warming by methane as a greenhouse gas, and
15 indirect contributions via production of other greenhouse gases (mainly tropospheric ozone) as it oxidizes to CO₂ in the atmosphere. Figure 3 compares the direct and indirect methane forcings from MAGICC and AM3, calculated via Eqs. (3) and (4), respectively. Each model attributes around 35-40% of methane's present-day total RF to indirect effects, and temporal patterns are consistent with each other (direct $r^2 = 0.87$; indirect $r^2 = 0.76$). The larger methane forcing in AM3 post-1950 is apparent in both the direct and indirect forcings, although the 2000-2005 decrease in RF is dominated by the indirect
20 component of the methane forcing (mostly tropospheric ozone). A time lag roughly on the order of methane's atmospheric lifetime (around 12 years) is present between the peaks and valleys of the AM3 direct and indirect methane forcings.

To build confidence in the simulation of surface air temperature by both MAGICC and CM3, we compare the model results with 20th Century reconstructions of surface air temperature, of which several independent datasets are available. Figure 4 shows the historical global-mean temperature responses to changes in all-forcings in MAGICC and CM3 compared with
25 NOAA and National Aeronautics and Space Administration (NASA) data, freely available online (<https://www.ncdc.noaa.gov/cag/time-series/global> and <https://data.giss.nasa.gov/gistemp/>). Following NOAA's methodology (NOAA, 2017), we compute the 20th Century average temperatures in MAGICC, CM3, and NASA, and calculate the annual temperature departures from this baseline. The two independent observational datasets are perfectly correlated ($r^2 = 1.00$). While MAGICC and CM3 both have high correlations with NOAA and NASA data, MAGICC has much higher correlation
30 coefficients (MAGICC $r^2 = 0.92$ (NOAA) and 0.93 (NASA); CM3 $r^2 = 0.75$ (NOAA) and 0.76 (NASA)). Consistent with Fig. 2, CM3 shows lower temperature responses post-1960 due to the strong effect of aerosols (Golaz et al. 2013). Overall, both



models adequately reproduce surface air temperature, providing confidence in both climate models of differing complexity levels.

The global mean surface air temperature responses attributed to CO₂ and methane forcings are shown in Fig. 5, calculated via Eqs. (1) and (2), respectively. The correlations of the ensemble-means are extremely high (CO₂ $r^2 = 0.98$; methane $r^2 = 0.92$).

5 Figure 5 also shows individual CM3 ensemble members and the range of MAGICC responses from all 19 AOGCM calibrations; however, we do not include MAGICC's highest climate sensitivity ensemble member as the responses were a clear outlier to the rest of the ensemble members.

We find that both CM3 and MAGICC attribute a nearly 1 °C rise in temperature from 1860 to 2014 from rising CO₂ concentrations (CM3: 0.9 °C; MAGICC: 0.9 °C). For methane, CM3 suggests a rise of 0.5 °C and MAGICC suggests a rise of
10 0.4 °C, consistent with the larger methane forcing in CM3 (Fig. 2). It is important to note that cooling from aerosols mask some of the warming that we otherwise would be experiencing from CO₂ and methane, which is why the combined warming from CO₂ and methane is larger than today's observed warming.

There are two major temperature response features in CM3 that are not present in MAGICC (Fig. 5). The first is a global mean cooling response to methane forcings around 1900 to 1915, which is strongly apparent in two of the three ensemble members.
15 Interestingly, this cooling response is not clearly reflected in the forcings of both the direct and indirect methane responses (Fig. 2). The second is a strong warming signal from 1980 to 1995, followed by cooling through 2000; this is consistent with AM3 RFs (Fig. 2) but more pronounced in the temperature signals.

Analyzing regional surface air temperature responses to CO₂ and methane isolated forcings (Fig. 6), shows that the methane-induced cooling between 1900 and 1915 is mostly attributed to the Southern Hemisphere and especially over Southern
20 Hemisphere oceans. This is likely due to the southern ocean polynya (Gordon and Comiso, 1988), which can be very strong in CM3, leading to very large unforced multidecadal time-scale variability over the southern ocean that propagates throughout the Southern Hemisphere (e.g., de Lavergne et al., 2014). On the other hand, the large methane warming in CM3 around 1990 is most prominent in the Northern Hemisphere, over both land and ocean.

When the global mean responses are parsed out by region (Fig. 6), the highest surface air temperature responses to methane
25 and CO₂ are found over land in the Northern Hemisphere, with temperatures from CO₂ rising by well over 1 °C from 1860 to 2014 in both models. There is high correlation between MAGICC and CM3 for all regions. We expect and find methane correlations between the two models to be slightly lower than CO₂ because methane has more complex chemical interactions in the atmosphere than CO₂ that introduce more degrees of freedom than CO₂, and are also potentially more simplified in MAGICC. We also find that correlations in the Southern Hemisphere are lower than in the Northern Hemisphere, especially
30 for methane.



An interesting feature present in the CM3 global mean and regional responses and not paralleled by MAGICC is that there are several time periods before 1950 when the methane temperature responses are comparable in magnitude to that by CO₂ (Fig. 5 and 6). We see this for all ensemble members, and it is consistent with AM3 RFs (Fig. 2). In the ensemble mean, the comparable warming magnitudes between 1940 and 1950 are consistent with the rate of growth of CO₂ concentrations slowing down while methane concentrations consistently increase (Fig. 1).

In contrast to the CO₂ and methane concentration trends from 1940-1950, the methane concentration growth rate slows down in the 1990s while the CO₂ concentrations consistently increase (Fig. 1). This is reflected in the CM3 temperature trends as a divergence in the magnitude of temperature responses between methane and CO₂ to where they stand in the present-day, with CO₂ yielding twice as much warming in 2014 as methane (Fig. 5).

A major difference between CM3 and MAGICC is the role of unforced variability in CM3. Ensemble member means and running averages are employed to dampen out variability, but it still plays a large role in decadal forcing and temperature responses. CM3, in particular, has been shown to produce magnitudes of variability on the upper end of CMIP5 models (Brown et al., 2015). To isolate the role of unforced variability in CM3, we plot a control simulation with constant preindustrial (1860) external radiative forcings for 500 years (Fig. 7). Temperature responses from unforced internal dynamics in CM3 introduce decadal temperature swings of 0.5 °C on average.

4 Conclusions

The purpose of this study is to enhance confidence in a freely available and computationally efficient reduced complexity climate model, MAGICC, in the context of simulating temperature responses to methane and CO₂ atmospheric concentrations. Our analysis is motivated by the need to determine a quick and accessible, yet reliable, method for analyzing impacts of future changes in methane emissions on climate warming. Given that sophisticated coupled climate-chemistry models are generally inaccessible and/or time-intensive and thus unavailable for analysis of methane mitigation strategies, employing a model like MAGICC, rather than relying on simple GWP metrics, would significantly enhance the accuracy of the assessment while still using basic infrastructure and meeting quick turnaround times.

To determine MAGICC's reliability for methane analysis, we performed four sets of experiments using MAGICC and CM3— all forcing with both time-varying natural and anthropogenic forcings but land-use held constant; simulations where CO₂ and methane concentrations are held constant at 1860 levels, respectively; and a simulation to isolate methane indirect effects resulting from its influence on ozone and water vapor (for MAGICC, we turned off methane chemistry; for CM3, we held methane radiative effects at 1860 levels).



Both CM3 and MAGICC models accurately reconstruct surface air temperature records from NOAA and NASA from 1860 through 2014, especially for 1950 onwards. For isolated forcings, MAGICC was able to adequately replicate CM3 temperature responses to methane and CO₂, including for indirect effects via methane chemical reactions. Correlation coefficients were very high at 0.98 and 0.92 in the global mean for CO₂ and methane, respectively, with overall magnitudes consistent. We therefore conclude that MAGICC is able to reproduce the isolated greenhouse gas forcing results of a more sophisticated coupled global climate model, providing confidence in the use of MAGICC for understanding the climate implications of methane mitigation analyses.

Further, we find that methane accounts for a considerable fraction of 20th Century and early 21st Century warming—roughly half that of CO₂'s warming response. However, there are some details captured by CM3 without parallels in MAGICC that suggest comparable warming contribution from both methane and CO₂ during the second half of the 20th Century. This is due to a larger direct and indirect methane forcing simulated by CM3 compared to MAGICC. CM3 also exhibits a range of unforced variability, not predicted by MAGICC. Whilst this acts as a hindrance to uncovering a forced signal, it also serves as a useful threshold for understanding the size of a forcing signal required for attribution. A good example of this is that CM3 exhibits a cooling response to methane from 1900 to 1915 likely due to the formation of southern ocean polynya leading to very large unforced multidecadal time-scale climate variability. More research is clearly needed to explore and evaluate these regional climate responses to increases in individual greenhouse gases.

Overall, we find that MAGICC, a reduced complexity climate model, is able to satisfactorily match the global mean temperature response to increases in greenhouses gases as simulated by the GFDL-CM3, a complex chemistry-climate model.

Code availability

- 20 The MAGICC v6 model is available for download at: <http://www.magicc.org/download> upon registration. The user manual can be accessed at: http://wiki.magicc.org/index.php?title=Manual_MAGICC6_Executable. Full model details along with nineteen sets of AOGCM-calibrated parameters used here for ensemble members are found in Meinshausen et al. (2011a). We update the default values of methane and tropospheric ozone radiative efficiency and methane atmospheric lifetime to values in Myhre et al. (2013).
- 25 The atmospheric model component (AM3) source code for GFDL CM3 is available here: <https://www.gfdl.noaa.gov/am3-model/>. The ocean model component (MOPM5) source code for GFDL CM3 is available here: <https://www.gfdl.noaa.gov/mom-ocean-model/>.



Data availability

Results from CM3/AM3 simulations and from the MAGICC model are available from Vaishali Naik (vaishali.naik@noaa.gov) and Ilissa Ocko (icko@edf.org), respectively, upon request.

Acknowledgements

- 5 Ilissa B. Ocko was funded by the Robertson Foundation and Heising-Simons Foundation. We thank Larry W. Horowitz for performing the long control simulation of CM3, and Alexandra Jones, Michael Winton, and Steven Hamburg for reviewing our manuscript.

References

- Allen, M. R., Fuglested, J. S., Shine, K. P., Reisinger, A., Pierrehumbert, R. T. and Forster, P. M.: New use of global warming potentials to compare cumulative and short-lived climate pollutants, *Nature Climate Change*, 6, 773–776, doi:10.1038/nclimate2998, 2016.
- Alvarez, R. A., Pacala, S. W., Winebrake, J. J., Chameides, W. L. and Hamburg, S. P.: Greater focus needed on methane leakage from natural gas infrastructure, *Proc. Nat. Acad. Sci.*, 109(17), pp.6435–6440, 2012.
- Austin, J., Horowitz, L. W., Schwarzkopf, M. D., Wilson, R. J. and Levy, H.: Stratospheric ozone and temperature simulated from the preindustrial era to the present day, *J. Clim.*, 26(11), pp.3528–3543, 2013.
- 15 Brown, P. T., Li, W. and Xie, S. P.: Regions of significant influence on unforced global mean surface air temperature variability in climate models, *J. Geophys. Res.: Atmos*, 120(2), pp.480–494, 2015.
- Collins, W. J., Lamarque, J. F., Schulz, M., Boucher, O., Eyring, V., Hegglin, M. I., Maycock, A., Myhre, G., Prather, M., Shindell, D. and Smith, S. J.: AerChemMIP: Quantifying the effects of chemistry and aerosols in CMIP6, *Geosci. Model Dev. Discuss.*, doi: 10.5194, 2016.
- 20 De Lavergne, C., Palter, J. B., Galbraith, E. D., Bernadello, R., and Marinov, I.: Cessation of deep convection in the open Southern Ocean under anthropogenic climate change, *Nature Clim. Change*, 4, 278–282, doi:10.1038/nclimate2132, 2014.
- Deser, C., Phillips, A., Bourdette, V. and Teng, H.: Uncertainty in climate change projections: the role of internal variability, *Clim. Dyn.*, 38(3–4), 527–546, doi:10.1007/s00382-010-0977-x, 2012.
- 25 Donner, L. J., Wyman, B. L., Hemler, R. S., Horowitz, L. W., Ming, Y., Zhao, M., Golaz, J. C., Ginoux, P., Lin, S. J., Schwarzkopf, M. D. and Austin, J.: The dynamical core, physical parameterizations, and basic simulation characteristics of the atmospheric component AM3 of the GFDL global coupled model CM3, *J. Clim.*, 24(13), 3484–3519, 2011.
- Etminan, M., Myhre, G., Highwood, E. J. and Shine, K. P.: Radiative forcing of carbon dioxide, methane, and nitrous oxide: A significant revision of the methane radiative forcing, *Geophys. Res. Lett.*, 43(24), 2016.



- Fiore, A. M., Naik, V., and Leibensperger, E. M.: Air quality and climate connections, *J. of Air & Waste Management*, 65:6, 645–685, doi: 10.1080/10962247.2015.1040526, 2015.
- Forster, P. M., Richardson, T., Maycock, A. C., Smith, C. J., Samset, B. H., Myhre, G., Andrews, T., Pincus, R. and Schulz, M.: Recommendations for diagnosing effective radiative forcing from climate models for CMIP6, *J. Geophys. Res. Atmos.*, 121(20), 2016.
- Griffies, S. M., Winton, M., Donner, L. J., Horowitz, L. W., Downes, S. M., Farneti, R., Gnanadesikan, A., Hurlin, W. J., Lee, H. C., Liang, Z. and Palter, J. B.: The GFDL CM3 coupled climate model: characteristics of the ocean and sea ice simulations, *J. Clim.*, 24(13), 3520–3544, 2011.
- Golaz, J.-C., Salzmann, M., Donner, L. J., Horowitz, L. W., Ming, Y., and Zhao, M.: Sensitivity of the aerosol indirect effect to subgrid variability in the cloud parameterization of the GFDL Atmosphere General Circulation Model AM3, *J. Clim.*, 24(13), doi:10.1175/2010JCLI3945.1, 2011.
- Gordon, A. L., and Comiso, J. C.: Polynyas in the Southern Ocean, *Sci. Amer.*, 256, 90–97, 1988.
- Guenther, A. B., Jiang, X., Heald, C. L., Sakulyanontvittaya, T., Duhl, T., Emmons, L. K. and Wang, X.: The Model of Emissions of Gases and Aerosols from Nature version 2.1 (MEGAN2. 1): an extended and updated framework for modeling biogenic emissions, *Geoscientific Model Development*, 5(6), 1471–1492, 2012.
- John, J. G., Fiore, A. M., Naik, V., Horowitz, L. W. and Dunne, J. P.: Climate versus emission drivers of methane lifetime against loss by tropospheric OH from 1860–2100, *Atmos. Chem. Phys.*, 12(24), 12021–12036, 2012.
- International Energy Agency (IEA): *World Energy Outlook*, 586, 2015.
- Lamarque, J. F., Bond, T. C., Eyring, V., Granier, C., Heil, A., Klimont, Z., Lee, D., Liousse, C., Mieville, A., Owen, B. and Schultz, M. G.: Historical (1850–2000) gridded anthropogenic and biomass burning emissions of reactive gases and aerosols: methodology and application, *Atmos. Chem. Phys.*, 10(15), 7017–7039, 2010.
- Lean, J. L.: Cycles and trends in solar irradiance and climate, *Wiley interdisciplinary reviews: climate change*, 1(1), 111–122, 2010.
- Levy, H. II, Horowitz, L. W., Schwarzkopf, M. D., Ming, Y., Golaz, J.-C., Naik, V. and Ramaswamy, V.: The roles of aerosol direct and indirect effects in past and future climate change, *J. Geophys. Res. Atmos.*, 118, 4521–4532, doi:10.1002/jgrd.50192, 2013.
- Lin, M., Fiore, A. M., Horowitz, L. W., Cooper, O. R., Naik, V., Holloway, J., Johnson, B. J., Middlebrook, A. M., Oltmans, S. J., Pollack, I. B. and Ryerson, T. B.: Transport of Asian ozone pollution into surface air over the western United States in spring, *J. Geophys. Res. Atmos.*, 117(D21), 2012.
- Meinshausen, M., Meinshausen, N., Hare, W., Raper, S. C. B., Frieler, K., Knutti, R., Frame, D. J. and Allen, M.R.: Greenhouse-gas emission targets for limiting global warming to 2°C, *Nature*, 458(7242), 1158, 2009.
- Meinshausen, M., Raper, S. C. B. and Wigley, T. M. L.: Emulating IPCC AR4 atmosphere-ocean and carbon cycle models for projecting global-mean, hemispheric and land/ocean temperatures: MAGICC 6.0, *Atmos. Chem. Phys.*, 8(2), 6153–6272, 2008.



- Meinshausen, M., Raper, S. C. and Wigley, T. M.: Emulating coupled atmosphere-ocean and carbon cycle models with a simpler model, *MAGICC6–Part 1: Model description and calibration*, *Atmos. Chem. Phys.*, 11(4), 1417–1456, 2011a.
- Meinshausen, M., Smith, S. J., Calvin, K., Daniel, J. S., Kainuma, M. L. T., Lamarque, J. F., Matsumoto, K., Montzka, S. A., Raper, S. C. B., Riahi, K., Thomson, A., Velders, G. J. M., and van Vuuren, D. P. P.: The RCP greenhouse gas concentrations and their extensions from 1765 to 2300, *Climatic change*, 109(1-2), 213, 2011b.
- 5 Meinshausen, M., Wigley, T. M. L. and Raper, S. C. B.: Emulating atmosphere-ocean and carbon cycle models with a simpler model, *MAGICC6–Part 2: Applications*, *Atmos. Chem. Phys.*, 11(4), 1457–1471, 2011c.
- Melvin, A. M., Sarofim, M. C., and Crimmins, A. R.: Climate Benefits of U.S. EPA Programs and Policies That Reduced Methane Emissions 1993–2013, *Environ. Sci. Technol.*, 50(13), 6873–6881, DOI: 10.1021/acs.est.6b00367, 2016.
- 10 Ming, Y., Ramaswamy, V., Donner, L. J. and Phillips, V. T.: A new parameterization of cloud droplet activation applicable to general circulation models, *J. Atmos. Sci.*, 63(4), 1348–1356, 2006.
- Myhre, G., Highwood, E. J., Shine, K. P., and Stordal, F.: New estimates of radiative forcing due to well mixed greenhouse gases, *Geophys. Res. Lett.*, 25, 2715–2718, 1998.
- Myhre, G., Shindell, D., Bréon, F.-M., Collins, W., Fuglestedt, J., Huang, J., Koch, D., Lamarque, J.-F., Lee, D., Mendoza, B., Nakajima, T., Robock, A., Stephens, G., Takemura, T., and Zhang, H.: Anthropogenic and Natural Radiative Forcing. In: *Climate Change 2013: The Physical Science Basis. Contribution of Working Group I to the Fifth Assessment Report of the Intergovernmental Panel on Climate Change* [Stocker, T.F., Qin, G.-K., Plattner, M., Tignor, S.K. Allen, J. Boschung, A. Nauels, Y. Xia, V. Bex and P.M. Midgley (eds.)], Cambridge University Press, Cambridge, United Kingdom and New York, NY, USA, 2013.
- 15 Naik, V., Voulgarakis, A., Fiore, A. M., Horowitz, L. W., Lamarque, J. F., Lin, M., Prather, M. J., Young, P. J., Bergmann, D., Cameron-Smith, P. J. and Cionni, I.: Preindustrial to present-day changes in tropospheric hydroxyl radical and methane lifetime from the Atmospheric Chemistry and Climate Model Intercomparison Project (ACCMIP), *Atmos. Chem. Phys.*, 13(10), 5277–5298, 2013.
- NOAA National Centers for Environmental Information, *Climate at a Glance: Global Time Series*, published May 2017, 25 retrieved on June 16, 2017 from <http://www.ncdc.noaa.gov/cag/>.
- Ocko, I. B., Hamburg, S. P., Jacob, D. J., Keith, D. W., Keohane, N. O., Oppenheimer, M., Roy-Mayhew, J. D., Schrag, D. P. and Pacala, S. W.: Unmask temporal trade-offs in climate policy debates, *Science*, 356(6337), 492–493, 2017.
- Ramanathan, V. and Xu, Y.: The Copenhagen Accord for limiting global warming: Criteria, constraints, and available avenues, *Proc. Nat. Acad. Sci.*, 107(18), 8055–8062, 2010.
- 30 Rayner, N. A., Parker, D. E., Horton, E. B., Folland, C. K., Alexander, L. V., Rowell, D. P., Kent, E. C. and Kaplan, A.: Global analyses of sea surface temperature, sea ice, and night marine air temperature since the late nineteenth century, *J. Geophys. Res. Atmos.*, 108(D14), 2003.
- Rogelj, J., McCollum, D. L., Reisinger, A., Meinshausen, M. and Riahi, K.: Probabilistic cost estimates for climate change mitigation, *Nature*, 493(7430), 79–83, 2013.



- Shindell, D. T., Faluvegi, G., Koch, D. M., Schmidt, G. A., Unger, N. and Bauer, S. E.: Improved attribution of climate forcing to emissions, *Science*, 326(5953), 716–718, 2009.
- Shindell, D., Kuylenstierna, J. C., Vignati, E., van Dingenen, R., Amann, M., Klimont, Z., Anenberg, S. C., Muller, N., Janssens-Maenhout, G., Raes, F. and Schwartz, J.: Simultaneously mitigating near-term climate change and improving human health and food security, *Science*, 335(6065), 183–189, 2012.
- Shine, K., Derwent, R., Wuebbles, D., and Morcrette, J.-J.: Radiative forcing of climate, in: *Climate Change: The IPCC Scientific Assessment*, edited by Houghton, J., Jenkins, G., and Ephraums, J., Cambridge University Press, New York, USA, 41–68, 1990.
- Shoemaker, J. K., Schrag, D. P., Molina, M. J. and Ramanathan, V.: What role for short-lived climate pollutants in mitigation policy?, *Science*, 342(6164), 1323–1324, 2013.
- Solomon, S., Daniel, J. S., Sanford, T. J., Murphy, D. M., Plattner, G.-K., Knutti, R., Friedlingstein, P.: Persistence of climate changes due to a range of greenhouse gases, *Proc. Natl. Acad. Sci.*; 107(43), 18354–18359, doi: 10.1073/pnas.1006282107, 2010.
- Stevenson, D. S., Young, P. J., Naik, V., Lamarque, J.F., Shindell, D. T., Voulgarakis, A., Skeie, R. B., Dalsoren, S. B., Myhre, G., Berntsen, T. K. and Folberth, G. A.: Tropospheric ozone changes, radiative forcing and attribution to emissions in the Atmospheric Chemistry and Climate Model Intercomparison Project (ACCMIP), *Atmos. Chem. Phys.*, 13(6), 3063–3085, 2013.
- Stocker, T. F., Qin, D., Plattner G.-K., Tignor, M., Allen, S. K., Boschung, J., Nauels, A., Xia, Y., Bex, V., Midgley, P. M.: *Climate Change 2013: The Physical Science Basis. Contribution of Working Group I to the Fifth Assessment Report of the Intergovernmental Panel on Climate Change*, Cambridge: Cambridge University Press, 2013.
- West, J. J., Smith, S. J., Silva, R. A., Naik, V., Zhang, Y., Adelman, Z., Fry, M. M., Anenberg, S., Horowitz, L. W., Lamarque, J.-F.: Co-benefits of mitigating global greenhouse gas emissions for future air quality and human health, *Nature Climate Change*, 3(10), 885–889, <http://doi.org/10.1038/NCLIMATE2009>, 2013.
- Wigley, T. M. L. and Raper, S. C. B.: Thermal-Expansion of Sea-Water Associated with Global Warming, *Nature*, 330, 127–131, 1987.
- Wigley, T. M. L. and Raper, S. C. B.: Implications for climate and sea level of revised IPCC emissions scenarios, *Nature*, 357, 293–300, 1992.
- Zhang, Y., Bowden, J. H., Adelman, Z., Naik, V., Horowitz, L. W., Smith, S. J. and West, J. J.: Co-benefits of global and regional greenhouse gas mitigation for US air quality in 2050. *Atmospheric Chemistry and Physics*, 16(15), 9533–9548, 2016.



	Experiments	Abbreviation	MAGICC v6	GFDL CM3
Direct Simulations	All-Forcing	AllForc	X	X
	CO ₂ concentrations held constant at 1860 levels	CO ₂ 1860	X	X
	CH ₄ concentrations held constant at 1860 levels	CH41860	X	X
	All-Forcing with CH ₄ chemistry turned off	CH4nochem	X	
	CH ₄ concentrations held constant at 1860 levels with CH ₄ chemistry turned off	CH41860nochem	X	
	CH ₄ held constant at 1860 levels for radiation only	CH4norad		X
Derived Simulations	CO ₂ -only		AllForc – CO ₂ 1860	
	CH ₄ -only		AllForc – CH41860	
	CH ₄ -direct		CH4nochem – CH41860nochem	AllForc – CH4norad
	CH ₄ -indirect		CH ₄ -only – CH ₄ -direct	CH4norad – CH41860

Table 1. Direct experiments performed by MAGICC and GFDL-CM3 models, as well as derived simulations. All-Forcing simulations include time-varying natural and anthropogenic forcings but land-use held constant. Each experiment is run for 19 ensemble members for MAGICC and three ensemble members for GFDL-CM3 over the period 1860 – 2014.

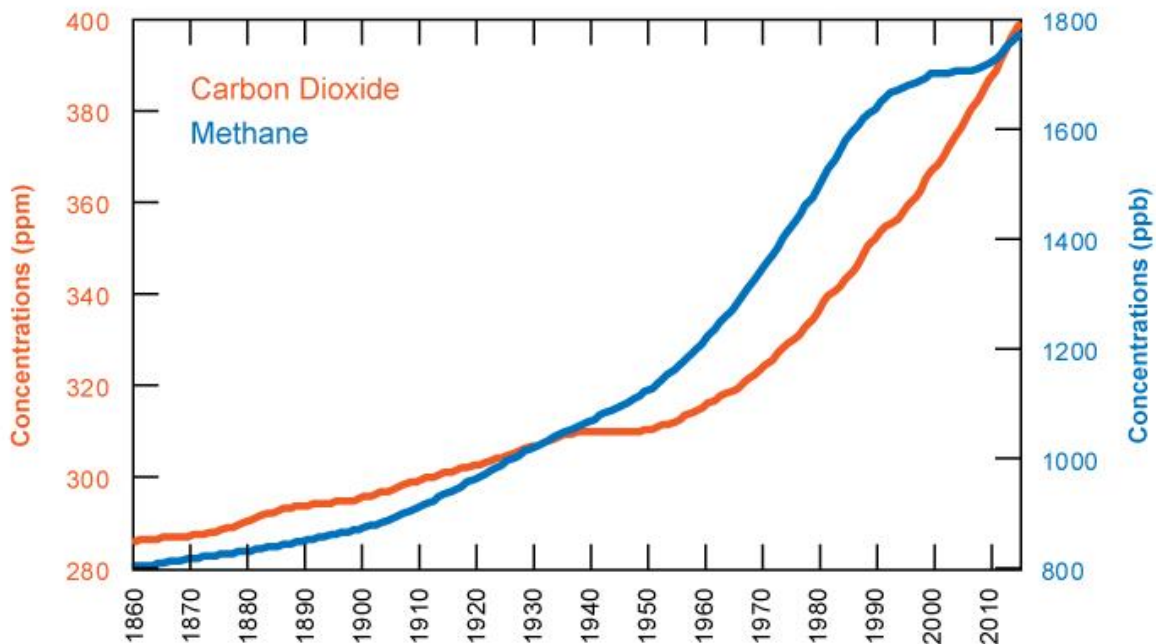
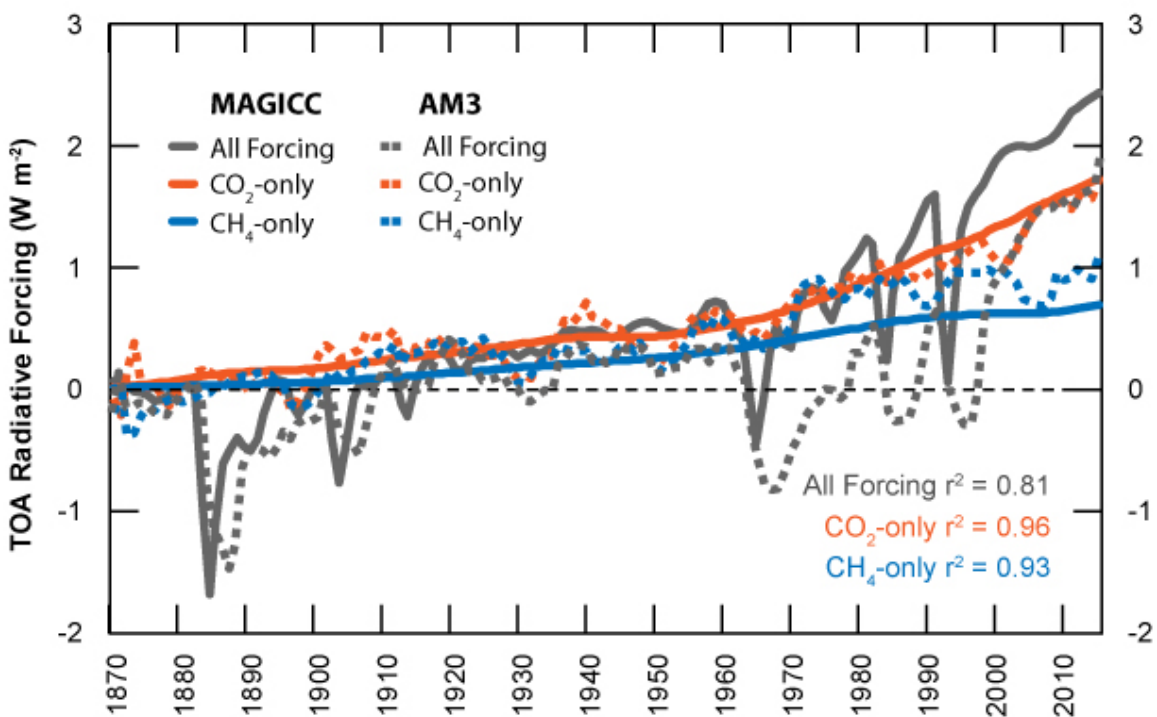
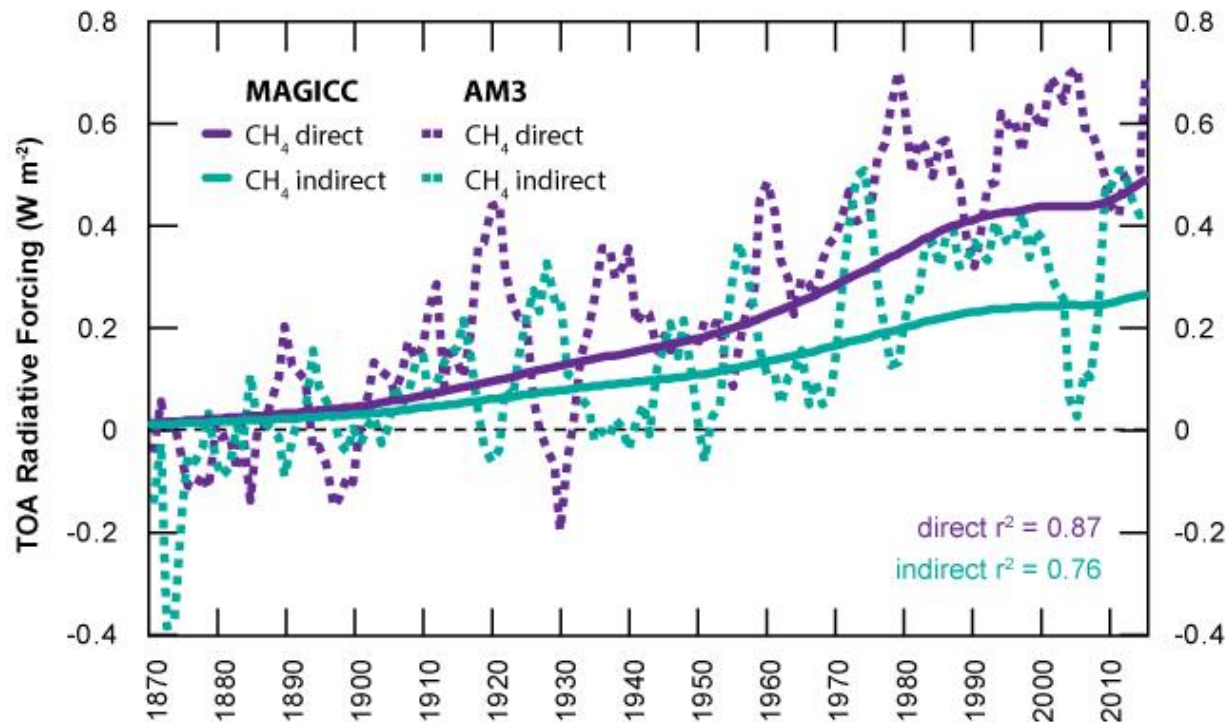


Figure 1. Atmospheric concentrations of carbon dioxide in parts per million (orange) and methane in parts per billion (blue) used in this study (Meinshausen et al. 2011b).



5 Figure 2. Top-of-atmosphere radiative forcings (W m^{-2}) after stratospheric adjustment due to all forcing (grey), CO_2 -only (orange), methane-only (blue), for both AM3 (dashed) and MAGICC (solid) model simulations. Methane forcing includes its direct as well as indirect effect from influences on chemistry. AM3 radiative forcings are technically ‘effective’ radiative forcings, and include tropospheric adjustments as well. AM3 data are 5-year running means. Correlation coefficients between MAGICC and AM3 radiative forcings are shown inset.



5 Figure 3. Direct (purple) and indirect (from methane's influence on ozone and water vapor, green) top-of-atmosphere radiative forcings (W m^{-2}) after stratospheric adjustment, for both AM3 (dashed) and MAGICC (solid) model simulations. AM3 radiative forcings are technically 'effective' radiative forcings, and include tropospheric adjustments as well. AM3 data are 5-year running means. Correlation coefficient between MAGICC and AM3 forcings are also shown.

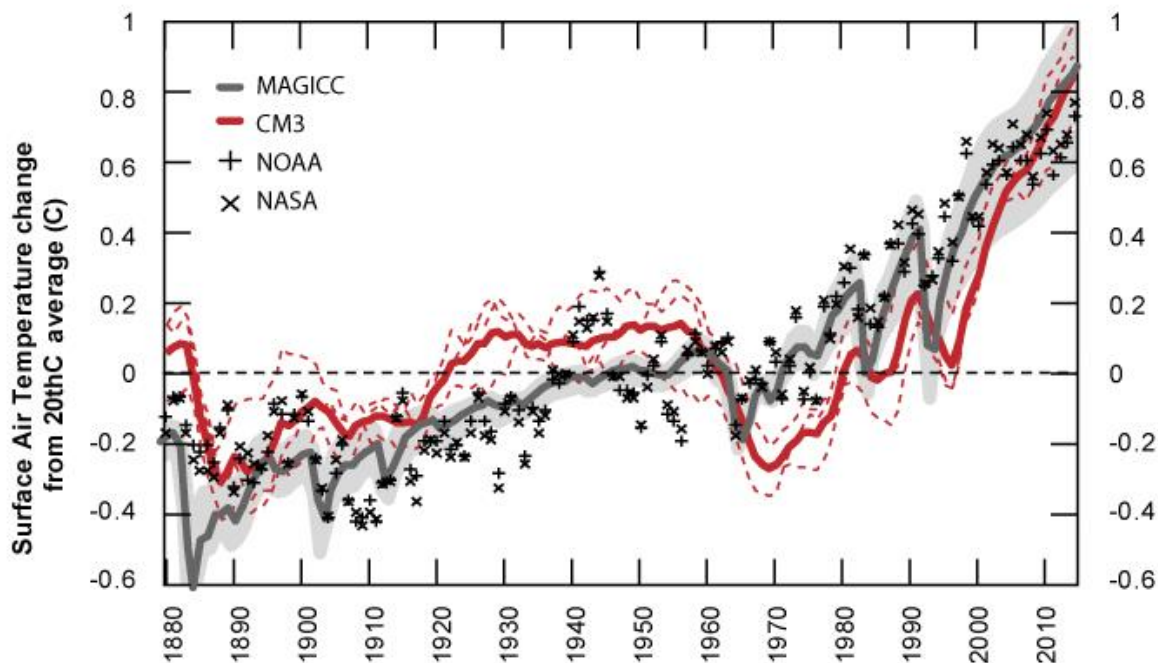


Figure 4. All forcing global-mean surface air temperature responses in °C for CM3 (solid red line) and MAGICC (solid grey line) model simulations as compared to observations by NOAA (+) (<https://data.giss.nasa.gov/gistemp/>) and NASA (x) (<https://www.ncdc.noaa.gov/cag/time-series/global>). All annual temperature anomalies shown as change from 20th Century average for each dataset. Individual ensemble members for CM3 runs shown in thin dashed red lines. Ensemble-member range for MAGICC shown as shaded grey. CM3 data are 5-year running means.

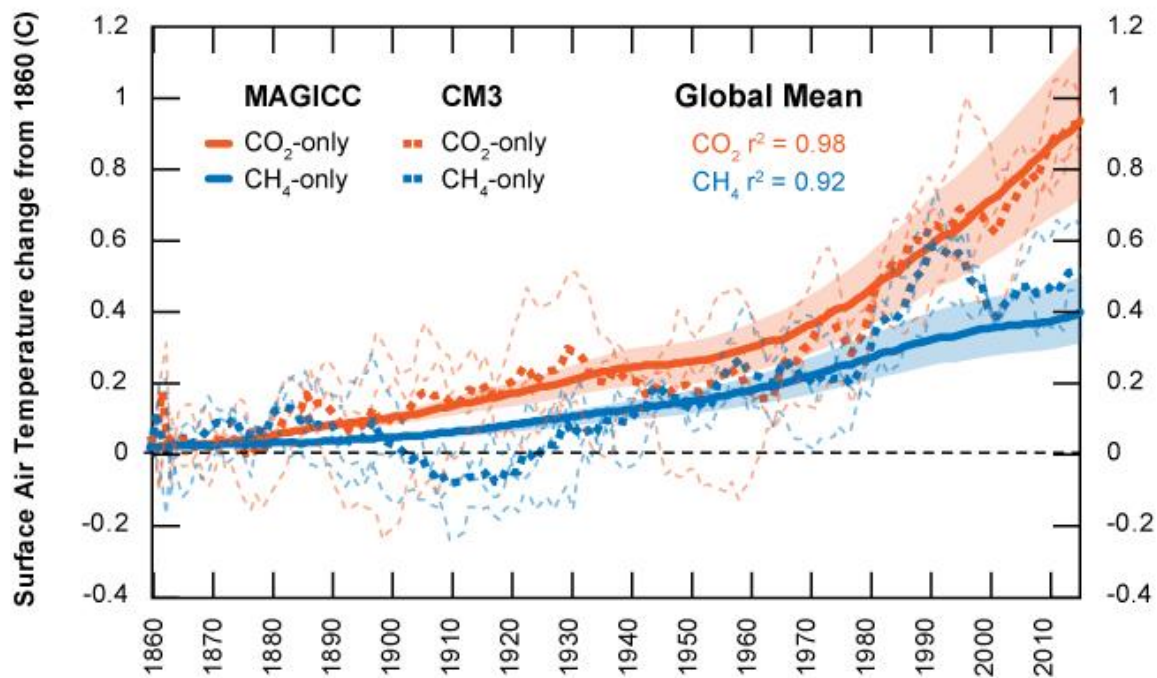
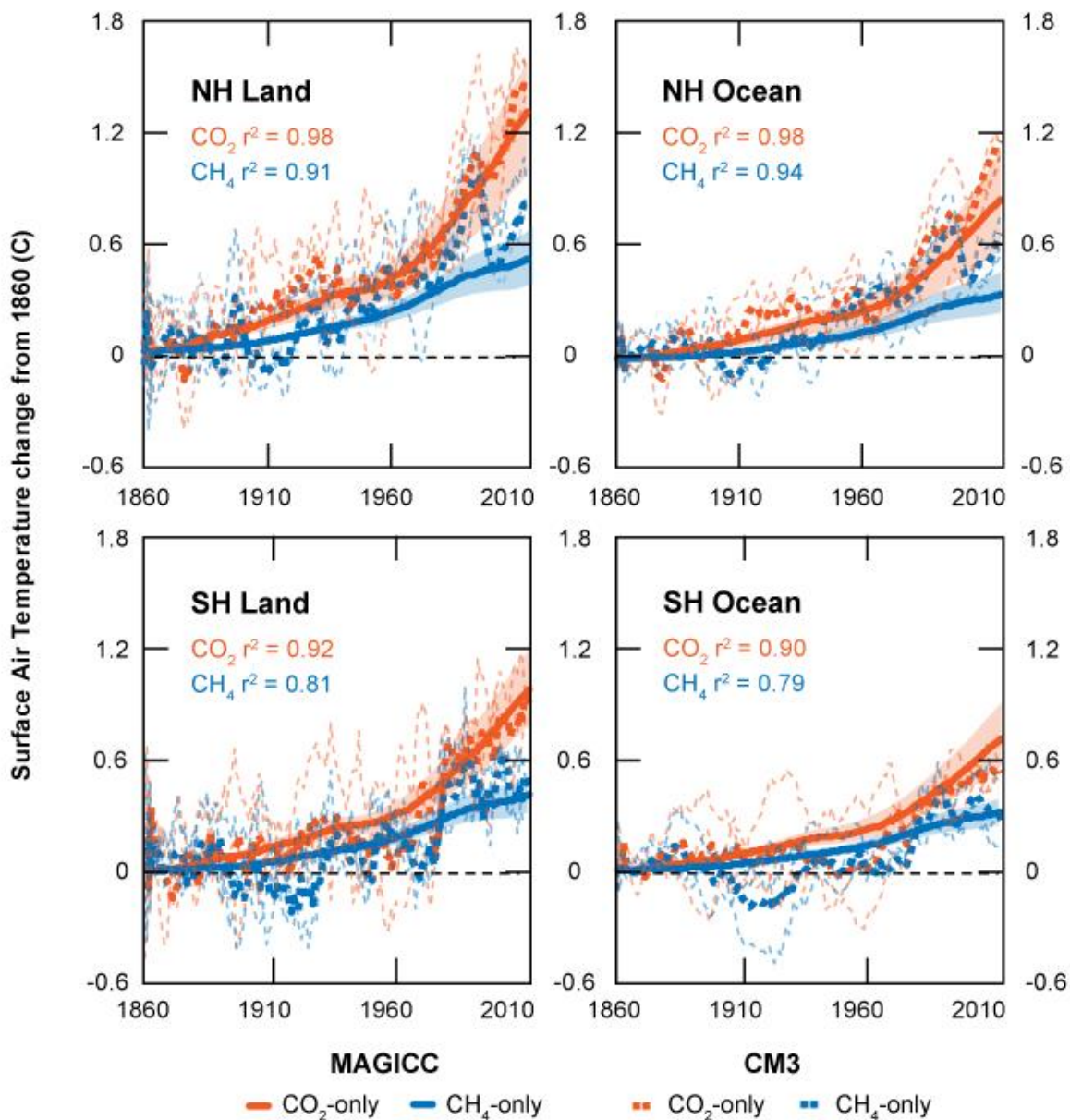


Figure 5. Global mean surface air temperature responses in °C for CM3 (dashed line) and MAGICCC (solid line) model derived simulations – CO₂-only (orange) and methane-only (blue). Individual ensemble members for CM3 runs shown in thin dashed lines. Range for MAGICCC ensemble-members shown in shaded colors. CM3 data are 5-year running means. Correlation coefficient
5 between MAGICCC and CM3 temperature responses are also shown.



5 Figure 6. Regional surface air temperature responses in °C for CM3 (dashed line) and MAGICCC (solid line) model indirect simulations – CO₂-only (orange) and methane-only (blue). Individual ensemble members for CM3 runs shown in thin dashed lines. Range for MAGICCC ensemble-members shown in shaded colors. CM3 data are 5-year running means. Correlation coefficient between MAGICCC and CM3 temperature responses are also shown.

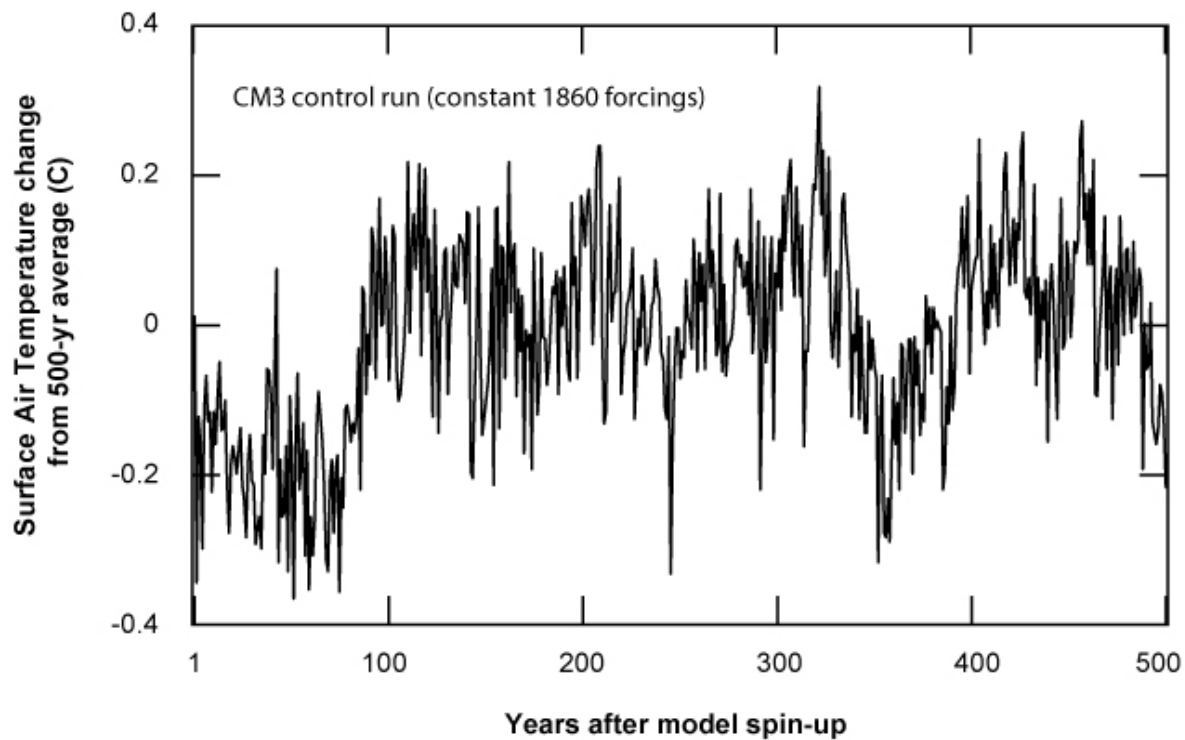


Figure 7. Surface air temperature fluctuations in °C introduced by unforced variability in CM3. Preindustrial (1860) forcings held constant with model run for 500 years post- 3000 year spin-up.